X-ray Structure and Microtubule Interaction of the Motor Domain of *Neurospora crassa* NcKin3, a Kinesin with Unusual Processivity[†,‡]

Alexander Marx,*[,§,||] Jens Müller,[§,||] Eva-Maria Mandelkow,[||] Günther Woehlke,[⊥] Cedric Bouchet-Marquis,[#] Andreas Hoenger,[#] and Eckhard Mandelkow[||]

Max-Planck-Unit for Structural Molecular Biology, Notkestrasse 85, 22607 Hamburg, Germany, Institute for Cell Biology, Ludwig-Maximilians-University Munich, Schillerstrasse 42, 80336, Germany, and Department of Molecular, Cellular, and Developmental Biology, University of Colorado, Boulder, Colorado 80309-0347

Received July 25, 2007; Revised Manuscript Received December 11, 2007

ABSTRACT: *Neurospora crassa* kinesin NcKin3 belongs to a unique fungal-specific subgroup of small Kinesin-3-related motor proteins. One of its functions appears to be the transport of mitochondria along microtubules. Here, we present the X-ray structure of a C-terminally truncated monomeric construct of NcKin3 comprising the motor domain and the neck linker, and a 3-D image reconstruction of this motor domain bound to microtubules, by cryoelectron microscopy. The protein contains Mg·ADP bound to the active site, yet the structure resembles an ATP-bound state. By comparison with structures of the Kinesin-3 motor Kif1A in different nucleotide states (Kikkawa, M. et al. (2001) *Nature (London, U.K.) 411*, 439−445), the NcKin3 structure corresponds to the AMPPCP complex of Kif1A rather than the AMPPNP complex. NcKin3-specific differences in the coordination of the nucleotide and asymmetric interactions between adjacent molecules in the crystal are discussed in the context of the unusual kinetics of the dimeric wild-type motor and the monomeric construct used for crystal structure analysis. The NcKin3 motor decorates microtubules at a stoichiometry of one head per $\alpha\beta$-tubulin heterodimer, thereby forming an axial periodicity of 8 nm. In spite of unusual extensions at the N-terminus and within flexible loops L2, L8a, and L12 (corresponding to the K-loop of monomeric kinesins), the microtubule binding geometry is similar to that of other members of the kinesin family.

Kinesins form a large superfamily that comprises molecules of different architecture and function, which have in common a high-homology catalytic domain or head, which is able to bind and hydrolyze ATP[1] and to interact with microtubules in a nucleotide-dependent manner (*1*, *2*). Most of the kinesins are motor proteins that use the energy from ATP hydrolysis for directed transport of various cellular cargoes. Conventional kinesin, the founding member of the Kinesin-1 family, is a dimeric motor protein, which moves processively along microtubules (*3*−*5*). While doing so, it hydrolyses one molecule of ATP per step in a strictly alternating way (*6*−*10*), suggesting that at any time, at least one head or motor domain is firmly attached to the microtubule. The hand-over-hand mechanism as a model of conventional kinesins processive movement is now well-supported by single molecule microscopy techniques with nanometer resolution (*11*−*15*) and high-resolution EM of microtubule-bound motor constructs (*16*), although it is still a matter of debate as to how the two heads are coordinated in detail (*17*).

Hand-over-hand walking is not the only mechanism used by kinesin motors to produce directed movement. The minus end directed C-type motor Ncd (Kinesin-14 family) seems to use a powerstroke mechanism that involves repetitive attachment and detachment of the motor (*18*−*20*). Keeping on track is not a problem for Ncd since this motor normally works in concert with many other Ncd molecules. Members of the Unc104/Kif1A family (Kinesin-3 family) are mostly monomeric, plus end directed motors (*21*, *22*), but still mouse Kif1A can move continuously along microtubules even as a single molecule (*23*). Instead of a second head, Kif1A and related motors use a family-specific, positively charged loop (K-loop) to prevent diffusion away from the microtubule surface by interaction with the negatively charged C-terminus of tubulin. This results in one-dimensional, biased Brownian diffusion along the microtubule (*23*). However, there is growing evidence that high local concentrations of Kinesin-3 motors lead to dimerization, causing the motors to switch from biased diffusion to more efficient processive hand-over-hand walking similar to conventional kinesin (*24*−*27*). Thus, it was surmised that dimerization is used as a means of regulating the transport accomplished by Kinesin-3 motors.

[†] This work was supported by the Deutsche Forschungsgemeinschaft (Grant MA563/8-3 to E.M.) and by the National Center for Research Resources of the National Institutes of Health (Grant 2P41RR000592 to A.H.).

[‡] The structure has been deposited in the PDB under ID 2OWM.

* To whom correspondence should be addressed. Tel.: +49 40 89984757; fax: +49 40 89716810; e-mail: marx@mpasmb.desy.de.

[§] A.M. and J.M. contributed equally to this work.

[||] Max-Planck-Unit for Structural Molecular Biology.

[⊥] Ludwig-Maximilians-University Munich.

[#] University of Colorado.

[1] Abbreviations: ATP, adenosine triphosphate; ADP, adenosine diphosphate; AMPPNP, adenosine 5′-[β,γ-imido]triphosphate; AMPPCP, adenosine 5′-[β,γ-methylene]triphosphate; NCS, non-crystallographic symmetry; MR, molecular replacement; EM, electron microscopy.

10.1021/bi701483h CCC: $40.75
Published on Web 01/19/2008

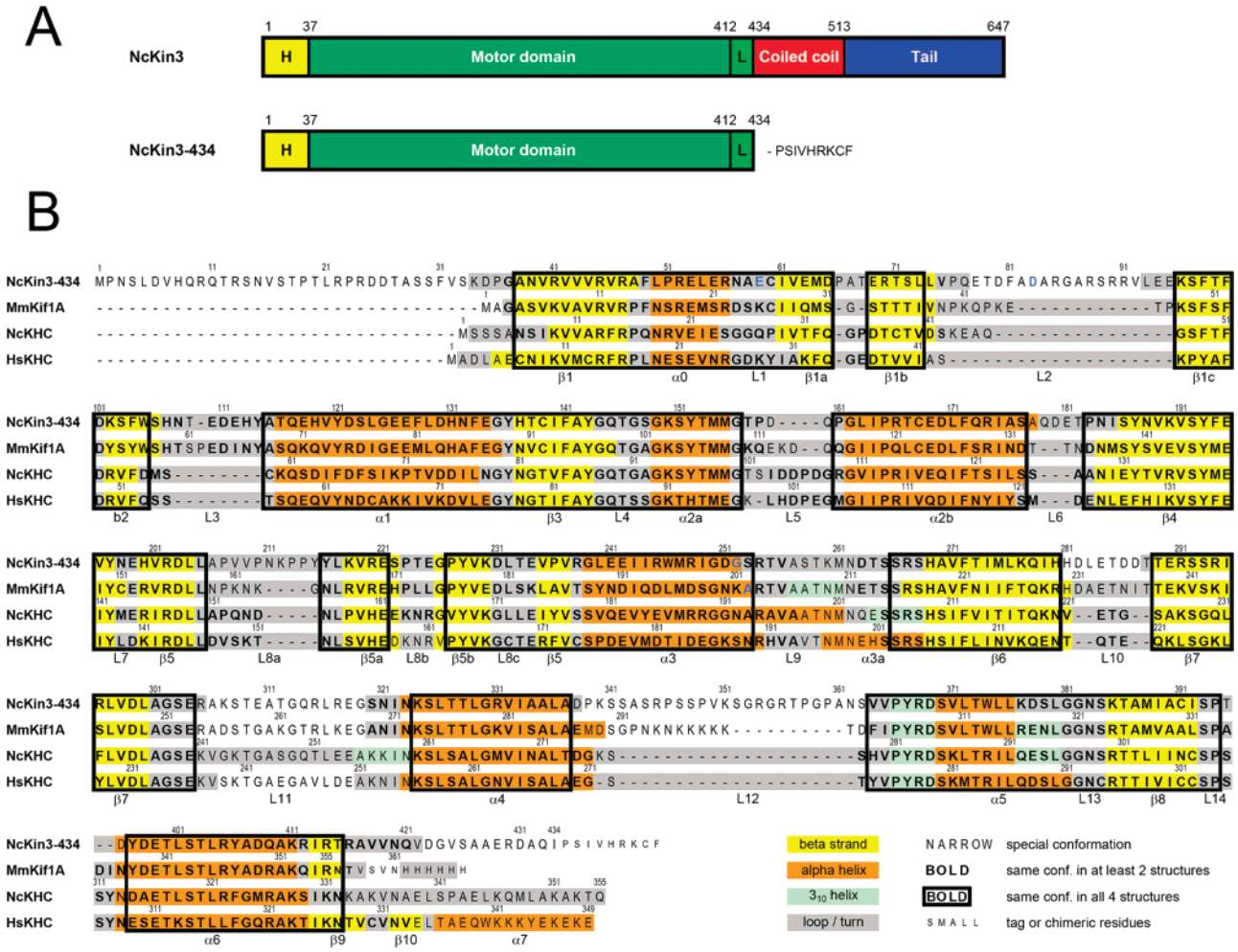

FIGURE 1: Domain structure and sequence alignment. (A) Domain structure of NcKin3 and the construct used for structural analysis. H: N-terminal extension of the motor domain (header) and L: neck linker. (B) Structure-based sequence alignment and secondary structure comparison with Kif1A and Kinesin-1 heavy chains. The sequences of four motor domain constructs with structures known by crystallographic analysis were first pre-aligned with ClustalW (*71*), and then the alignment was manually corrected and optimized by superpositon of the 3-D structures and rearrangement of misaligned residues according to their local conformational similarities. Residue ranges of similar conformations in all four structures are in bold and boxed in black lines. Residues outside the boxes that are printed in bold indicate similar conformations in only two or three structures; in most of these cases, the two Kinesin-1 and/or the two Kinesin-3 structures are similar. White background indicates disordered regions. Secondary structure assignments were calculated with Procheck (*59*, *72*). Naming of the structural elements follows the convention introduced for rat Kinesin-1 heavy chain (*40*) with only minor modifications (e.g., the last segment of the bulky insertion in strand β5 is now explicitly labeled L8c). Sequences and structures used for alignment are as follows: NcKin3: the sequence of NcKin3-434 (this work) is identical to the UniProt sequence Q9C2M3, except that the first 29 N-terminal residues are missing (Met1 of NcKin3-434 corresponds to Met30 of Q9C2M3) and that three residues (blue letters) differ (NcKin3-434 Glu59, Asp83, and Gly252 correspond to Lys88, Asn112, and Arg281 in Q9C2M3). The first 434 residues of NcKin3 are followed by an unrelated sequence of 9 residues (Cys-tag, PSIVHRKCF). Molecule A was used for structural alignment and secondary structure assignments. MmKif1A: chimeric construct of Kif1A from mouse (UniProt P33173, residues 1−355, Pro202 engineered to Ala) followed by 6 residues of the neck linker of Kif5C and a His_6-tag; alignment based on the structure of the Mg-AMPPNP complex: PDB− ID 1i6i (*31*). NcKHC: *N. crassa* Kinesin-1, UniProt P48467; structure of the ADP complex: PDB ID 1goj (*43*). HsKHC: *Homo sapiens* ubiquitous Kinesin-1 heavy chain, UniProt P33176; structure of the ADP complex crystallized with Li_2SO_4: PDB ID 1mkj (*42*).

Neurospora crassa NcKin3 is a member of a fungal-specific subgroup of small Kif1A-related motors (*28*) that are characterized by an unusually short C-terminal part beyond the motor domain (Figure 1A). Its normal cellular function remains to be elucidated, but it is probably involved in mitochondria movements. In cells defective of Nckin2, another *Neurospora* Kinesin-3 motor that is essential for the interaction of mitochondria with microtubules, NcKin3 is upregulated, and mitochondria lacking NcKin2 require NcKin3 for binding to microtubules in vitro (*29*). In contrast to other Kinesin-3 members, NcKin3 forms native dimers; hence, in this case, dimerization is not used for regulation (*30*). Another surprising result from the analysis of NcKin3's ATPase activity is that only one subunit releases ADP in a microtubule-dependent manner, suggesting a non-processive powerstroke mechanism similar to Ncd.

Much of our knowledge about the mechanisms used by kinesin motors to convert chemical free energy into directed motion relies on atomic models derived by crystal structure analysis, combined with high-resolution image reconstructions of motor-microtubule complexes (*24*, *31*−*38*). Structures of motor domains from representatives of several kinesin families are now available, including conventional kinesins from various species (*39*−*43*), C-type motors such as Ncd and Kar3 (*20*, *44*−*48*), and the monomeric Kinesin-3 family member Kif1A (*31*, *32*). The general folding being

the same in all known structures, valuable insight could be gained by comparing structures of motor domains from different sources and in different nucleotide binding states (for a review, see ref *49*). Two switch regions surrounding the nucleotide were identified, which are most important in acting and reacting to nucleotide hydrolysis and in translating and amplifying local conformational changes in the active center into large scale effects. Depending on the nucleotide state, switch I containing the NxxSSR motif seems to melt and transform between a helical and a hairpin-like conformation, inducing changes in position, orientation, and length of helix α3 at the long edge of the central β-sheet (*32*, *46*). Switch II connects via a flexible loop to the switch II helix (α4) or switch II cluster (including surrounding elements: loop L12, helix α5, and loop L13), which control the central docking site of the neck linker (*50*) and coordinate the large scale conformational changes required for directed motion along the microtubule. Loop L11, which is highly flexible according to the crystal structures (i.e., in the absence of microtubules) is supposed to assume a rigid conformation in the microtubule-kinesin complex (*31*) and thus may act as a clutch that couples or uncouples in a microtubule-dependent manner the nucleotide binding state to the switch II helix (relay helix) and hence to the neck linker and neck. This hypothesis is corroborated by a recent 9 Å resolution cryo-EM analysis of the nucleotide-free microtubule-kinesin complex that provided direct evidence for a microtubule-induced rearrangement of loop L11 accompanied with an elongation of the switch II helix (*38*).

Most of the structures determined by X-ray crystallography were obtained from motor domains with ADP in the active site. Regarding the position and orientation of the switch II cluster, essentially two classes of conformations can be distinguished: one with a docking site for the neck linker between the switch II cluster and the core of the motor domain (permissive conformation, as in human conventional kinesin structure 1mkj (*42*)) and another one without such a site, where the switch II cluster prevents docking of the neck linker (obstructive conformation, as in human conventional kinesin structure 1bg2 (*39*)). On the basis of models derived from atomic structures of single motor domains and EM images of microtubule-kinesin complexes, the obstructive conformation is thought to represent the ADP-bound state, while the permissive state is assumed to be similar to the ATP-bound state (*37*). In the case of mouse Kif1A, structures of complexes with different ATP analogues are available, which allows modeling of the mechanochemical cycle in more detail (*31*, *32*). One conclusion from the comparison of X-ray structures in different nucleotide states is that in the absence of microtubules, the conformation is not fully determined by the nucleotide bound in the active center (*51*).

The amino acid sequence of NcKin3, *N. crassa*'s small version of a Kinesin-3 motor, differs from that of mouse Kif1A not only in having a short stalk-tail domain. There are numerous changes, mostly within the loop regions connecting well-conserved secondary structure elements in the motor domain (Figure 1B). The most obvious differences in the primary structure are as follows: (i) Unlike Kif1A and other typical N-type kinesins, the conserved motor domain is preceded by a long extension of about 35 amino acids. The function of the NcKin3-specific header is unclear, and a truncated construct lacking the N-terminal extension has unchanged microtubule-stimulated ATPase activity (*30*). (ii) In Kif1A and other typical Kinesin-3 family members, loop L12 (K-loop) contains a cluster of positively charged lysines. In NcKin3, the corresponding loop is about twice the size of the K-loop in Kif1A. It does not contain a cluster of lysines but a similar number of positively charged residues (two lysines and three arginines), which are almost equally spaced along the loop. (iii) The sequence of amino acids between β1 and β2 of the central β-sheet forms a subdomain consisting of helix α0 and a small three-stranded β-sheet: β1a, -b, -c. Loop L2 between β1b and β1c varies considerably in length and shape between different types of kinesin. Kinesin-3 family members possess rather long L2 loops, in general (nine residues in Kif1A). In NcKin3, this loop is much expanded and consists of about 20 amino acids. Here, we present the crystal structure of a C-terminally truncated construct of NcKin3 that spans the N-terminal header, the core motor domain, and the neck linker, as well as its complex with microtubules obtained by cryoEM. Although the header and some loop regions (including the previously mentioned loops L2 and L12) are mostly disordered in the crystal, comparison of the structure with other kinesins, especially with Kif1A in different nucleotide states, revealed unexpected details. These are discussed in the context of the unusual kinetic behavior that NcKin3 exhibits in dimerization and microtubule-stimulated ATPase activity (*30*).

EXPERIMENTAL PROCEDURES

Expression and Purification of Recombinant NcKin3 Motor Domain. The cloning of the plasmid pNcKif434, a pT7-7 derivative, is described elsewhere (*30*). The coded protein comprises the conserved motor domain of NcKin3, the following 14 amino acids, and a Cys-tag (amino acids PSIVHRKCF (*52*)). The polypeptide NcKin3-434 is 434 + 9 residues long and has a size of 49.5 kDa. The protein was expressed in *Escherichia coli* strain BL21 STAR. Cells grown in 6 L of LB media supplemented with 50 mg/L ampicillin were induced at $A_{600} = 0.6-1.0$ with 0.4 mM isopropyl-β-D-thiogalactopyranoside (IPTG) for 16 h at 24 °C. Packed cells were resuspended in lysis buffer (50 mM PIPES, pH 6.9, 1 mM EGTA, 1 mM $MgCl_2$, 1 mM DTT, 50 mM NaCl, 2 mM benzamidine, and 0.5 mM PMSF). Lysates were prepared using a French press cell. The expressed motor protein fragment was purified by two cation-exchange columns (phosphocellulose and MonoS) using NaCl to elute the protein. The NcKin3 fragment containing fractions were pooled, concentrated, and applied to a gel filtration column (G200 Hiload 16/60). The column was equilibrated with 50 mM phosphate, pH 7.5, 1 mM $MgCl_2$, 1 mM EGTA, 1 mM DTT, 150 mM NaCl, and 50 μM ATP. Peak fractions were pooled and concentrated to about 10 mg/mL.

Crystallization and X-ray Data Collection. Crystallization was performed by the hanging drop method. Crystals suitable for X-ray diffraction were obtained by mixing 1.5 μL of protein solution with 0.5 μL of reservoir (0.1 M HEPES, pH 7.5, 0.2 M sodium potassium tartrate, 24% PEG3350) and 0.2 μL of 0.1 M $MgCl_2$. X-ray data were collected at the synchrotron beamline X13 at DESY, Hamburg, Germany. Prior to crystal freezing for data collection, the crystals were transferred into a buffer containing 25% PEG3350 and 5% glycerol as the cryoprotectant. Cryoprotected crystals were

Table 1: Data Reduction and Refinement Statistics[a]

params	values
space group	$P2_1$
unit cell	$a = 75.9$ Å, $b = 98.4$ Å, $c = 111.8$ Å, $\beta = 91.9°$
Data collection	
resolution (last shell) (Å)	3.25 (3.31−3.25)
no. of observations $>1\sigma$	99727
no. of unique reflns	26085
completeness, overall (last shell) (%)	100 (100)
R_{sym}, overall (last shell)	0.143 (0.705)
$\langle I\rangle/\langle\sigma(I)\rangle$, overall (last shell)	9.8 (1.9)
Refinement and modeling	
resolution limits (Å) overall (last shell)	111.8−3.25 (3.334−3.250)
no. of reflns, working set (test set)	24775 (1329)
no. of non-hydrogen atoms in the model	10337
no. of NcKin3-434·ADP·Mg^{2+} complexes	4
total no. of residues	1772
total no. of residues modeled	1308
total no. of residues in NCS groups	1300
no. of NCS groups	3
NCS restraints (in all groups)	tight positional, tight thermal
R_{work}, overall (last shell)	0.210 (0.256)
R_{free}, overall (last shell)	0.272 (0.327)
av B factor (Å^2)	76.1
rms Deviation from ideal values	
bond lengths (Å)	0.018
bond angles (deg)	1.845

[a] $R_{sym} = \sum_{hkl}\sum_i|I_i - \langle I\rangle|/\sum_{hkl}\sum_i\langle I\rangle$, where I_i is the ith measurement of symmetry equivalent reflection intensities, and $\langle I\rangle$ is the weighted mean of all measurements I_i. $R_{work} = \sum_{hkl}||F_{obsd}| - |F_{calcd}||/\sum_{hkl}|F_{obsd}|$, where F_{obsd} and F_{calcd} are the observed and calculated structure factors, and the summation is over the working set (95% of all reflections). R_{free} is calculated accordingly with summation over the remaining 5% of reflections (test set) not used for refinement.

exposed to X-rays in a stream of cold nitrogen gas. Since no additional nucleotide was supplied during crystallization and the nucleotide in the stock solution was hydrolyzed to ADP due to the basal ATPase activity of the construct, the crystals contained ADP in the active site.

Structure Determination. The crystals belonged to space group $P2_1$ with $a = 75.9$ Å, $b = 98.4$ Å, $c = 111.8$ Å, and $\beta = 91.9°$ and diffracted to about 3.25 Å resolution (Table 1). Data reduction and statistical analysis was performed with Denzo and Scalepack (HKL data processing system V1.97.2 (*53*)). The averaged intensities were converted and truncated to amplitudes using programs of the CCP4 suite (*54*). The structure was solved by molecular replacement using Phaser version 1.2 (*55*) with a search model derived from the structure of the KIF1A motor domain complexed with ADP (PDB− ID 1i5s) and assuming four NcKin3-434 molecules per asymmetric unit (Matthews coefficient 2.11 Å^3/Da). The model was refined using the programs Refmac5 (*56*) and Coot (*57*). Composite omit maps of partially refined models were calculated with CNS 1.1 (*58*). Procheck (*59*) and Whatcheck (*60*) were used to check the geometry of the model. During refinement, tight positional and thermal noncrystallographic symmetry (NCS) restraints were used. At the beginning, a single NCS group for all four molecules was applied. During the final stages of refinement, four NCS groups were used to allow for some obvious differences due to nonequivalent crystal contacts: one for the core residues and three separate NCS groups for some surface regions according to the similarities of their environment (see Figure 2).

3-D Analysis of Microtubule-NcKin3-434 Complexes. Monomeric NcKin3-434 protein was incubated with preformed microtubules for 2 min at room temperature (for a protocol see, ref *61*). The buffers used were BRB80 (80 mM PIPES, 100 mM NaCl, 2 mM $MgCl_2$) supplemented with 5% DMSO and 2 mM AMPPNP (Sigma, St. Louis, MO) as a nonhydrolyzable ATP substitute. DMSO was used to enhance the formation of helical 15-protofilament microtubules during polymerization to facilitate the structural analysis (30 min at 37 °C).

EM. Immediately after incubation of motors and microtubules, the specimens were plunge-frozen in liquid ethane (*62*) and imaged with a GATAN-914 cryo-holder at a nominal magnification of 50 000*x* in a Tecnai-F20 field-emission electron microscope (FEI-Company, Eindhoven, The Netherlands). Data were recorded on Kodak SO-163 film plates. The film plates were scanned at 2000 dots per inch with a Nikon-Coolscan 9000ED. After initial rotations and straightening, the data were further binned by a factor of 2 to compensate for interpolation artifacts. This resulted in a final pixel (voxel) size on the electronic data of 0.508 nm with respect to the actual specimen size.

Helical 3-D Analysis. Images were screened for microtubules composed of 15 protofilaments that exhibited a right-handed supertwist (see refs *61* and *63*). Only these microtubules can be used as a helical template. For a recent introduction into helical analysis of motor-microtubule complexes, see ref *63*. Briefly, for helical reconstruction, we used the software packages PHOELIX (*64*) that was specifically modified for this purpose and SUPRIM (*65*). 3-D volumes were visualized with Volvis (SUNY, Stonybrook, NY). Molecular docking of the X-ray map into the EM scaffold was performed with UCSF-CHIMERA (*66*).

RESULTS

General Description of the NcKin3-434 Crystal Structure. A construct consisting of residues 1−434 of the NcKin3 sequence (plus nine residues from the C-terminal Cys-tag, PSIVHRKCF) was crystallized in the presence of magnesium and ADP and analyzed by X-ray crystallography. The Cys-tag consists of a fragment of *Dictyostelium* actin 15 gene (*52*), which is known to react with maleimide and other thiol-reactive agents and which had been used for biotinylation of the NcKin3 motor domain. This construct, NcKin3-434, comprises an N-terminal header of 36 amino acids, the motor domain (residues 37−412), and the neck linker (residues 413−434, Figure 1). The crystal contains four crystallographically independent molecules (A−D, Figure 2). The resolution of X-ray diffraction data was only 3.25 Å, limited by the quality of the crystals (Table 1). Despite the modest resolution, the derived model is reliable because tight NCS restraints for all four molecules were applied throughout refinement. In this way, the number of free parameters could be reduced considerably. Furthermore, the refined model showed clear deviations from the structure that was used for molecular replacement and exhibited unanticipated similarities to another structure, ruling out a severe bias toward the MR model and over-interpretation of the data. The header

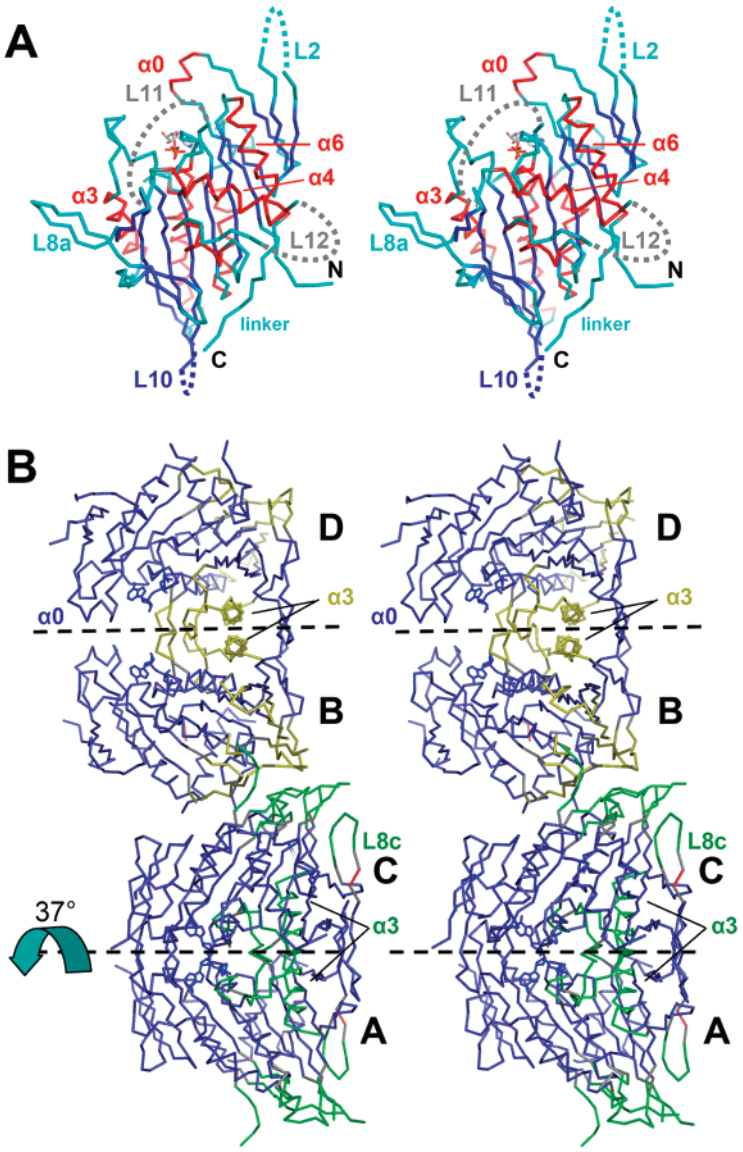

FIGURE 2: C_α trace of NcKin3-434 (stereoview). (A) Overview of molecule A in the standard orientation, with main structural elements labeled, viewed from the microtubule surface onto the microtubule binding surface of the motor domain. In this orientation, the microtubule plus end would point to the bottom of the page. The nucleotide is indicated near L11 in the upper part of the structure, and the switch II cluster (helix α4 and surrounding structural elements) is located in the middle. Note that the C-terminal linker is docked onto the body of the motor domain (bottom right). Helices are shown in red, *β*-strands in blue, and loops in cyan; missing loops are indicated by dotted lines. (B) Contents of the asymmetric unit with four independent molecules. Molecules A and C and molecules B and D form pairs with 2-fold rotational pseudo-symmetry. The two pairs can be superimposed by translation and rotation of one pair by about 37° around its pseudo-symmetry axis. However, the superposition is not perfect, indicating significant variations at the surface regions. Noncrystallographic symmetry groups used at the end of the refinement are indicated by different colors: blue: 237 residues (per molecule) mostly in the core of the structure that are considered equivalent in all four molecules; green: 88 residues that are considered equivalent in A and C, but different to B and D; and yellow: a similar set of residues considered to be equivalent in B and D but different to A and C. Eight residues in total, mostly at the termini or in flexible loops, were not subjected to NCS restraints (red). Figure was prepared with Pymol (*73*).

and the C-terminus beyond residue 422 were not visible in the structure, similarly to about 60 residues of each molecule in loops L2, L10, L11, and L12. Because of weak electron density for some side chains, 11 residues at the surface were modeled as alanines. In total, the model covers about 74% of the protein content in the crystals, and it includes four complexes of ADP·Mg^{2+} in the nucleotide binding pockets.

Conformation of the Motor Domain. Apart from minor effects induced by different crystal contacts, the structures of the four molecules are almost identical. As an ADP state conformation was expected, initial phases were calculated by molecular replacement starting from the structure of the ADP complex of chimeric KIF1A (*31*), a KIF1A construct comprising the catalytic domain, the neck linker, and a His-tag with part of the neck linker replaced by the corresponding part of conventional mouse kinesin (hereafter called KIF1A). The first electron density map (Figure 3) already showed clear differences between NcKin3-434 and the model structure, especially within the switch regions, switch I (α3-L9-α3a, in KIF1A) and switch II (α4-L12-α5-L13). Superposition of the final structure with the structures of KIF1A in complex with ADP or AMPPCP revealed that NcKin3-434 resembles the AMPPCP complex (*31*) rather than the ADP complex, although ADP is bound in the nucleotide binding pocket. The similarity covers the important structural elements that are directly involved in the mechanism of

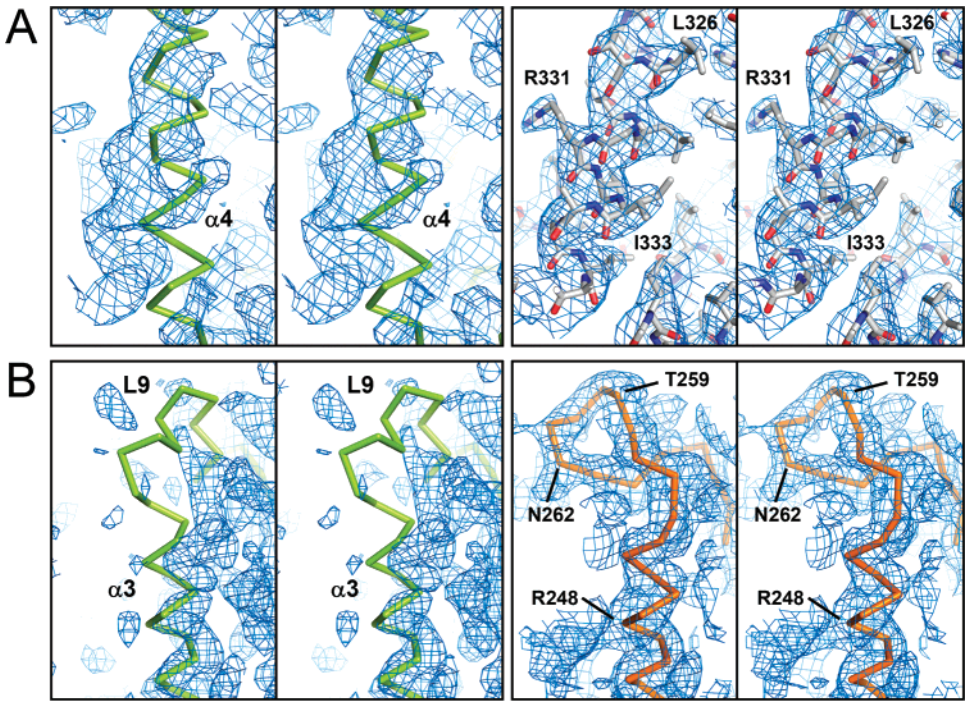

FIGURE 3: Electron density maps of the switch regions. Stereoviews of NCS averaged electron density maps around (A) helix α4 and (B) helix α3 and loop L9. The stereo pairs at the left side show the initial unrefined map after MR phasing using a truncated model derived from the structure of the Kif1A complex with ADP (PDB ID 1i5s (*31*)). The unrefined map clearly indicates that the conformation of the NcKin3 structure differs from that of Kif1A·ADP in both switch regions. The C_α traces in green show the position and conformation of the switch elements in the Kif1A·ADP structure (not included in the search model). The stereo pairs at the right side show the NCS average of the final map, in overlay with the refined structure of NcKin3 in stick representation (A) and as a C_α trace (B) to avoid overcrowding. The refined structure closely resembles the Kif1A complex with AMPPCP (PDB− ID 1i6i (*31*)) both in the switch I and the switch II region (see Figures 4 and 6). From the comparison of the two maps at the left and the right side, it is obvious that this unexpected similarity is not due to a bias toward the search model. Figure was prepared with Pymol (*73*).

kinesin's motile activity: the switch I region (helix α3 and the sequence leading to β6, in its entirety called loop L9 in the following, irrespective of its special conformation), the switch II cluster, and the neck linker.

Switch I Region. In most of the ADP containing structures, loop L9 is partially helical, and the helical part usually overlaps with the switch I motif NxxSSR (for a review, see ref *49*). Although there is considerable conformational variability between the different types of kinesin motor domains, the ADP complex of Kif1A is still predominantly helical in loop L9 and roughly similar to conventional kinesin in this region (Figure 4). In the AMPPCP containing structure of Kif1A, the loop adopts a hairpin-like conformation. The transition from the ADP-bound to the AMPPCP-bound conformation induces a slight rotation of helix α3. In the ADP-bound structure of NcKin3-434, the switch I region is most similar to that of the Kif1A·AMPPCP complex, both in the hairpin-like conformation of loop L9 and in the position of helix α3. The latter is remarkable because the position of helix α3 is obviously not affected by its interaction with the neighboring molecule (Figure 5; there is no such interaction between the molecules in the Kif1A crystal). The structures are not only similar in the folding of the backbone but also in side chain conformations, especially within the switch I motif. The orientation of serine S266/215 (NcKin3/Kif1A), for instance, which plays an important role in ATP hydrolysis, is equivalent in both structures (see Discussion).

Switch II Cluster. By definition, the switch II cluster extends from helix α4 to loop L13 at the N-terminus of helix α6 and includes loop L12 between α4 and heavily distorted helix α5. NcKin3 differs from other members of the Kinesin-3 family by an ample loop L12 (~25 residues), which is almost twice as long as the K-loop (L12) in Kif1A. Furthermore, it does not contain the characteristic cluster of six lysine residues, which is thought to interact with the negatively charged surface of microtubules and might be important for the processive movement of single headed kinesins (*67*); however, L12 does contain a similar number of five basic residues spread out evenly that might fulfill the same function. As in Kif1A, this loop is almost completely disordered. The remaining part of the switch II cluster (α4, α5, and L13) has very much the same conformation and position in NcKin3-434 and in the AMPPCP complex of Kif1A (Figure 6C). Thus, the core of the switch II cluster is not much affected by the presence or absence of a long insert between α4 and α5, at least in the crystal environment, lacking the interaction with the microtubule surface.

Neck Linker. Comparing the available structures of kinesin motor domains (*49*), the switch II cluster toggles between two conformational states ("up" and "down"). In the up conformation (Figure 6C), a binding groove is opened between the switch II cluster and the central β-sheet (β1), which allows the neck linker to dock to the core motor domain (permissive conformation). This conformation is expected for the ATP state (*37*). The down or obstructive conformation (Figure 6D) prevents docking of the neck linker and is considered to be the generic conformation of the ADP state, although exceptions from this rule exist (e.g., rat and human KHC structures 2kin and 1mkj (*40*, *42*)). In the

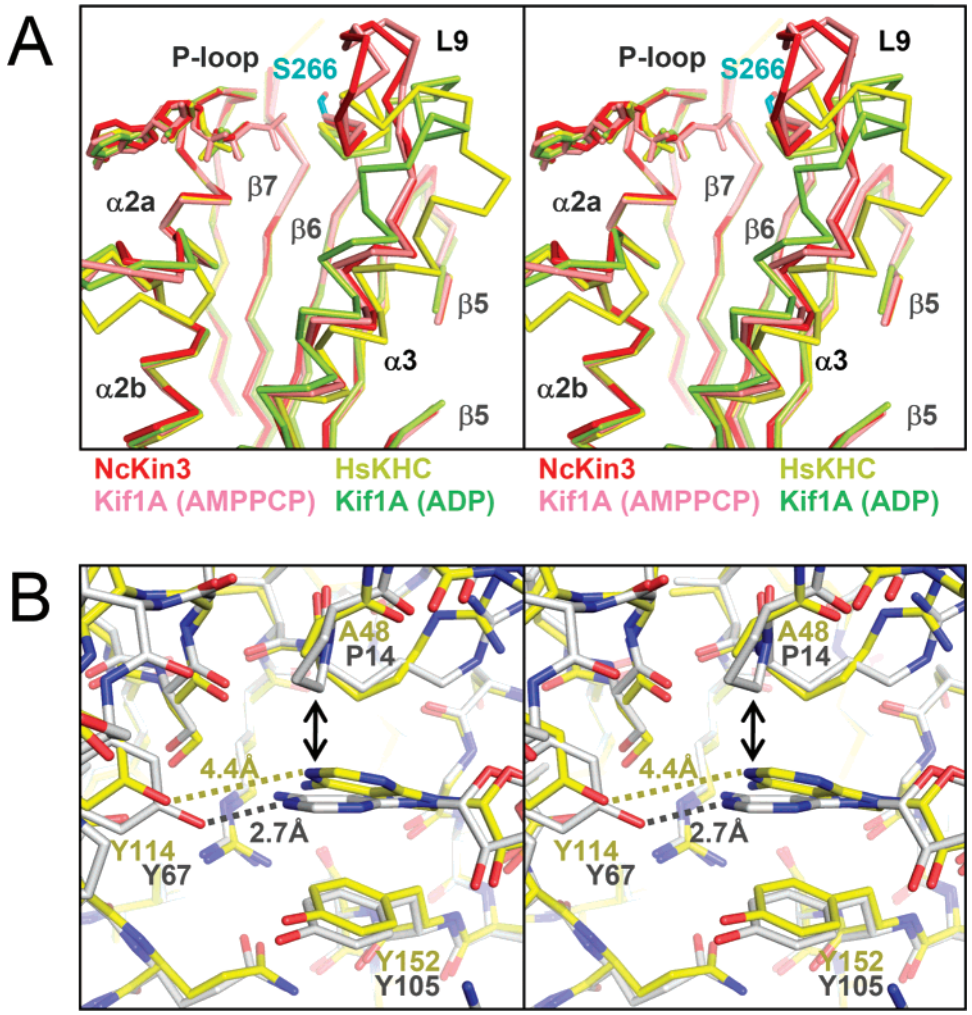

FIGURE 4: Switch I region and nucleotide binding. (A) Stereoview showing the nucleotide binding site (P-loop) and the switch I region (helix α3 and loop L9) of the NcKin3 structure in superposition with those of MmKif1A in complex with AMPPCP or ADP (PDB IDs 1i6i and 1i5s (*31*)) and human KHC with ADP (PDB− ID 1mkj (*42*)). Serine S266 of NcKin3 is highlighted as a marker for the position of the switch I motif (NxxSSR) at the end of loop L9. The overlay was calculated by least-squares fitting of the P-loop region (using residues I140−M154 in NcKin3 and the corresponding residues of the other structures). There is a striking similarity in the position of α3 and the fold of loop L9 between NcKin3 (red) and the structure of mouse Kif1A when complexed with the ATP analogue AMPPCP (pink), although the NcKin3 structure has ADP bound in the nucleotide binding pocket. By contrast, the α3 helices of the ADP containing structures of Kif1A and HsKHC are slightly tilted (in opposite directions) from the position in NcKin3, while the conformation of loop L9 of Kif1A·ADP seems intermediate to Kif1A·AMPPCP/NcKin3·ADP on the one side and HsKHC·ADP on the other side. (B) Close-up view of the nucleotide binding site with the adenine moiety shown in the center; overlay of NcKin3 (yellow carbon atoms) with MmKif1A in complex with AMPPCP (gray carbon atoms). Proline P14 (MmKif1A) in the highly conserved RxRP binding motif is replaced by an alanine (A48) in NcKin3. This exchange allows the adenine moiety to move up, toward the alanine, which results in disruption of a hydrogen bond with the side group of Y114 and in weakening of the stacking interaction between adenine ring system and Y152. Figure was prepared with Pymol (*73*).

structure of the NcKin3-434·ADP complex, switch II is in the up position, corresponding to the ATP state, and the neck linker is docked. Similar to other ATP-like structures (*50*), isoleucine I413 at the beginning of β9 plays a central role in the docking interaction (Figure 6D): its side group points to the interior and fits into a hydrophobic pocket formed by residues of the switch II cluster (I333, L336, and L380), the central β-sheet (V40 and F141), and the end of helix α6 (A410).

In molecules A and C of the NcKin3-434 structure, the linker is further stabilized in the docked conformation by arginine R414. With its long side chain, R414 binds to a sharp bend formed by the N-terminal extension of the motor domain. Docking of the neck linker, however, does not depend on this interaction since the neck linker in molecules B and D has a similar conformation without such reinforcement. The neck linker is almost completely docked and aligns roughly parallel to the edge of the core β-sheet, approaching β7 at the tip of the motor domain, while in the Kif1A structure with AMPPCP the neck linker is only semi-docked: the C-terminal part beyond β9 is mostly disordered. (Note that the Kif1A construct used as a comparison was a chimera and that the neck linker sequence was partially replaced by the corresponding sequence of mouse KHC (*31*).)

Nucleotide Binding. The P-loop residues and nucleotides of the NcKin3 structure fit very well to those of the other structures, except that the adenine base in the NcKin3 structure was rotated by about 20° relative to the adenine plane of the other molecules (Figure 4). This can be explained by an unusual alanine (A48) in the NcKin3 sequence, which replaces the highly conserved proline of the adenine binding motif RxRP (Figure 4B). As a consequence of the rotation,

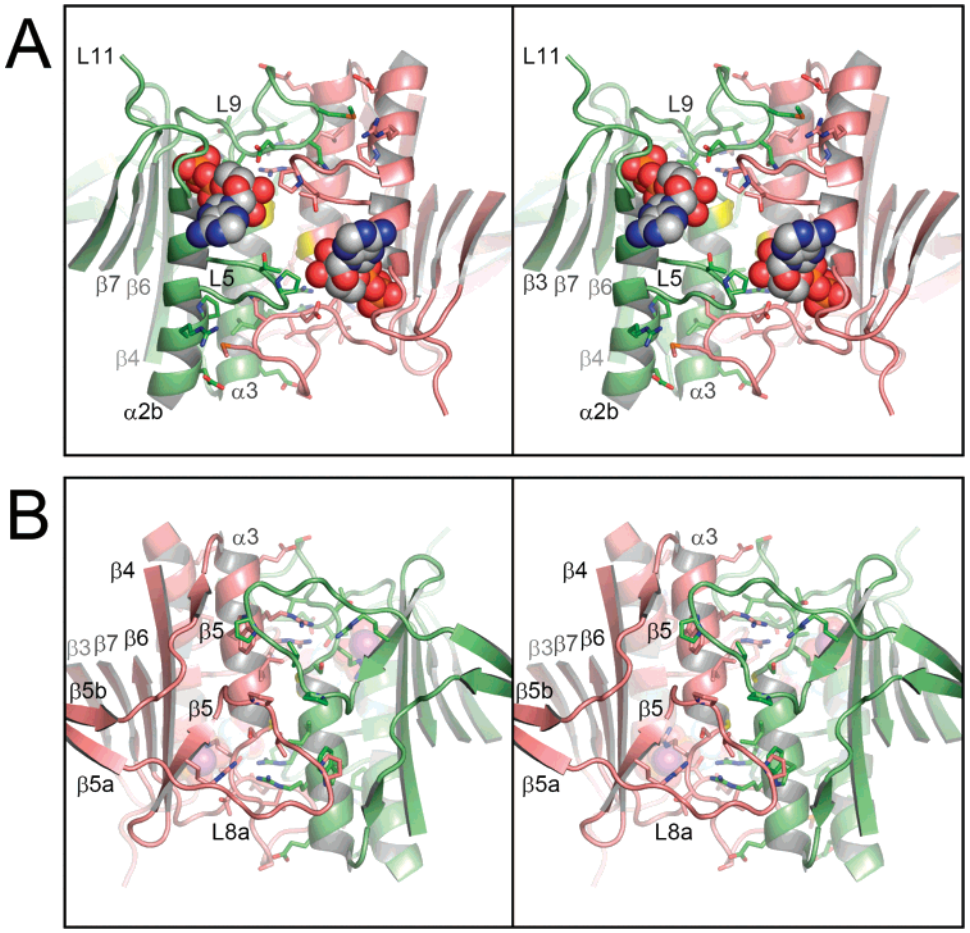

FIGURE 5: Pseudo-symmetric interaction of the switch I region. Stereoview of the interacting zones of molecules A (green) and C (salmon) with surrounding structural elements shown as ribbons, ADP and magnesium as spheres, and side groups of residues with intermolecular distances below 4 Å as sticks. (A) Helices α3 are in antiparallel orientation and staggered, such that glycines Gly252 at the ends of the helices (yellow patches of the helical ribbon) are at a short distance to each other ($C_\alpha - C_\alpha$ distance is 4.7 Å). Because of the stagger, helix α3 of one molecule is mostly interacting with loop L9, the C-terminal extension of α3, of the other molecule. In addition, L9 of one molecule also interacts with helix α2b and the α2 insert L5 of the other molecule. The nucleotides are in close proximity to each other, and the minimal distance between the 2′-oxygens is 8.7 Å. Remarkably, the 3′-OH groups of the ribose moieties are at a hydrogen bonding distance to the carboxyl groups of Asp159 of the interacting molecule. (B) View after rotation by 180°. The mostly hydrophobic, proline-rich loop L8a, which is enlarged by 4−5 residues as compared to Kif1A and human KHC, associates with its counterpart by alignment of their LAPVVP segments (residues 205−210).

tyrosine Y114 (in the loop preceding helix α1) is not within hydrogen-bonding distance to the adenine base as the corresponding Y67 in the Kif1A structures, and the stacking interaction between the adenine ring system and the tyrosine Y152 is weakened.

Interactions between Molecules. In the crystal, molecules A and C interact strongly and 180° symmetrically with each other, and so do molecules B and D (Figure 5). The pairing is mainly due to close packing of the switch I regions (helices α3 and the following loop L9) at the center of the contact region. Two other regions contribute to this symmetric interaction: (i) Loop L5, a short insert of six amino acids in the middle of helix α2, interacts with loop L9 of the companion molecule and (ii) the enlarged loop L8a of the L8-*β*5a,b lobe interacts with its counterpart in the other molecule. The two pseudo-symmetric pairs (A, C) and (B, D) are almost equivalent. The rms distance of the C_α atoms after least-squares superposition of the two pairs is 1.1 Å (as compared to ∼0.1 Å between individual molecules of the same pair and ∼0.5 Å between molecules of different pairs). The slightly elevated rms value between the pairs is due to a scissor-like relative movement of the molecules.

There is another type of strong interaction between pairs of molecules in the crystal. The asymmetric pairs [B, C] and [D, A′] (squared brackets indicate that the order matters) are also very similar to each other, even more so than the symmetric pairs: the rms difference of C_α atoms after superposition of the asymmetric pairs is only 0.27 Å. Remarkably, the [B, C] type pairing involves a relative rotation of 144° bringing the neck linkers of both molecules in close contact with each other (Figure 6). The neck linkers run almost perpendicular to each other and meet close to their C-terminal ends, so that the main chain oxygen of Q421 in B can form a hydrogen bond with the backbone nitrogen of V419 in C. Since dimerization of full-length NcKin3—as in the case of conventional kinesin (*41*)—is based on a coiled-coil interaction of the neck helices (*30*), the neck linkers of the two protomers have to converge to form a dimer. Thus, the asymmetric pairs of molecules in the crystal structure could serve as a plausible model for the contacts that are formed in the true NcKin3 dimer between the two heads. This is even more suggestive if one considers the fundamental asymmetry of dimeric NcKin3, which can hardly be explained by coiled-coil interactions alone (see Discussion).

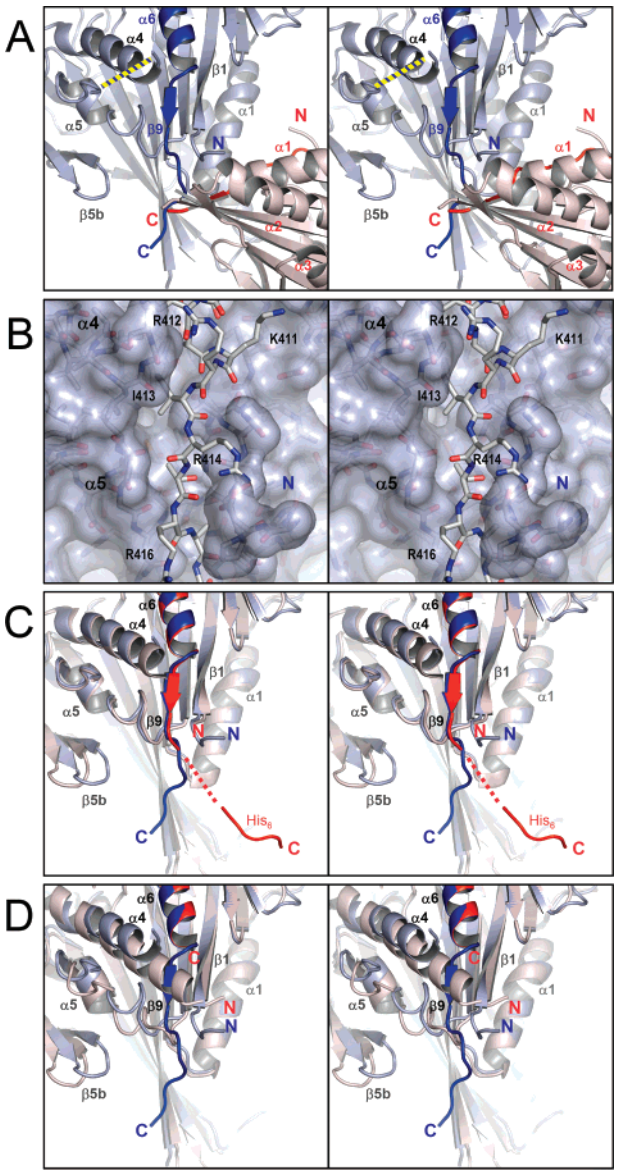

FIGURE 6: Interactions of the neck linker. Stereoviews of the neck linker and its interaction with surrounding structures. (A) Ribbon diagram of two molecules (red: B and blue: C) that interact by direct contact of their neck linkers. The linkers (as far as modeled) and the preceding helices α6 are drawn in saturated colors. N- and C-termini of the modeled part of the structure are labeled. In both molecules, the N-terminal extension of the motor domain is missing due to disorder. The model of molecule B starts with Ala38 at the beginning of strand *β*1. The model of molecule C comprises four more residues N-terminally to *β*1; these residues form a sharp bend, approaching helix α2a and loop L6 of molecule B. The neck linker (*β*9 up to the C-terminus of the visible structure) runs from the end of helix α6 toward loop L10 at the tip of the molecule, which is partially disordered. The line in yellow and blue indicates 25 missing residues of loop L12 between α4 and α5. (B) Stick model of molecule C in the same orientation as in panels A, C, and D; enlarged view of the region around *β*9 (Ile413-Arg414-Thr415). Lys411 marks the end of helix α6. The molecule except helix α6 and the neck linker is shown within a transparent envelope. The linker fits into a groove formed by α4, α5, *β*8, and *β*1 (docked conformation). The side chain of Arg414 hooks into the bend formed by the residues at the N-terminus. (C and D) Overlays of molecule C with the structures of mouse KIF1A with Mg-AMPPCP (C, PDB− ID 1i6i) and Mg-ADP (D, PDB− ID 1i5s). The conformation of linker and docking groove of NcKin3 (with Mg-ADP) is virtually identical to that of KIF1A complexed with the ATP analogue. Figure was prepared with Pymol (*73*).

However, the NcKin3 construct that was crystallized is too short for dimerization in solution (*30*), and the residues beyond D423 (B) and V422 (C) are disordered in the crystal structure. Thus, the relevance of the asymmetric pairing in the crystal remains somewhat speculative.

NcKin3-Microtubule Complex. Helical 3-D reconstruction of NcKin3-434-microtubule complexes was performed in the presence of AMPPNP (Figure 7A,B). A total of 20 independent data sets (near and far sides of 10 intact microtubules varying in length between ∼300 and 900 nm) corresponding to about 20 000 asymmetric units was averaged. Fourier diffraction of unprocessed images and an averaged dataset of 15-protofilament microtubules (Figure 7A) revealed layerline ratios that indicate a close to stoichiometric motor-tubulin dimer decoration (data not shown); hence, most of the motor-binding positions on microtubules are filled so that the 3-D map reproduces an accurate shape of the motor head domains and their attachment to tubulin subunits. Phase−amplitude plots of selected layerlines (e.g., see ref *63*) show reliable data to approximately 2.5 nm resolution (see Supporting Information figure). Docking the X-ray structure of NcKin3-434 and the electron crystallographic structure of α*β*-tubulin (*68*) revealed the interface between motor head and tubulin dimer in high molecular detail (Figure 8). The major mass of the kinesin head is superimposed on *β*-tubulin, but as kinesin is more extended than a tubulin subunit (∼6 nm, as compared with tubulin's 4 nm), it overlaps with the α-tubulin subunits on the minus end side along the tubulin protofilament. Although between the docked structures there is a wide gap between the minus end directed part of the kinesin head and the underlying α-tubulin surface (Figure 8B), the EM density between these elements suggests that it may host parts of the extended loop 2 (Figure 8B), which is not visible in the X-ray structure. There are also free densities at the predicted locations of loops 11 and 12 (Figure 8A). Structural details are further analyzed in the Discussion.

DISCUSSION

Nucleotide State and Overall Conformation. The NcKin3-434 construct was crystallized without additional nucleotides from the protein of a 10 mg/mL stock solution (∼200 *μ*M) that contained the motor-bound nucleotide and a small amount of ATP (50 *μ*M), which is hydrolyzed to ADP due to the basal activity of the construct (0.004 s^{-1} (*30*)). Accordingly, crystal structure analysis revealed clear electron density for ADP, indicating that the majority of the molecules had ADP bound at the nucleotide binding site. Nevertheless, the structure exhibited features typical for an ATP-like nucleotide state. As compared to the structures of mouse Kif1A, another motor of the Kinesin-3 family, in various nucleotide states (*31*, *32*), the similarity is most pronounced with the AMPPCP-bound structure.

According to ref *32*, the Kif1A structure with AMPPCP represents the collision complex or pre-isomerization state, by contrast to the AMPPNP complex, which corresponds to the pre-hydrolysis state. In transition to the presumed pre-hydrolysis state, the highly conserved serine S215 at the end of loop L9 flips toward the nucleotide, so that it can interact with the *γ*-phosphate. At the same time, loop L9, which has a hairpin-like structure in the KIF1A·AMPPCP complex (Figure 4), melts and becomes partially disordered. Consider-

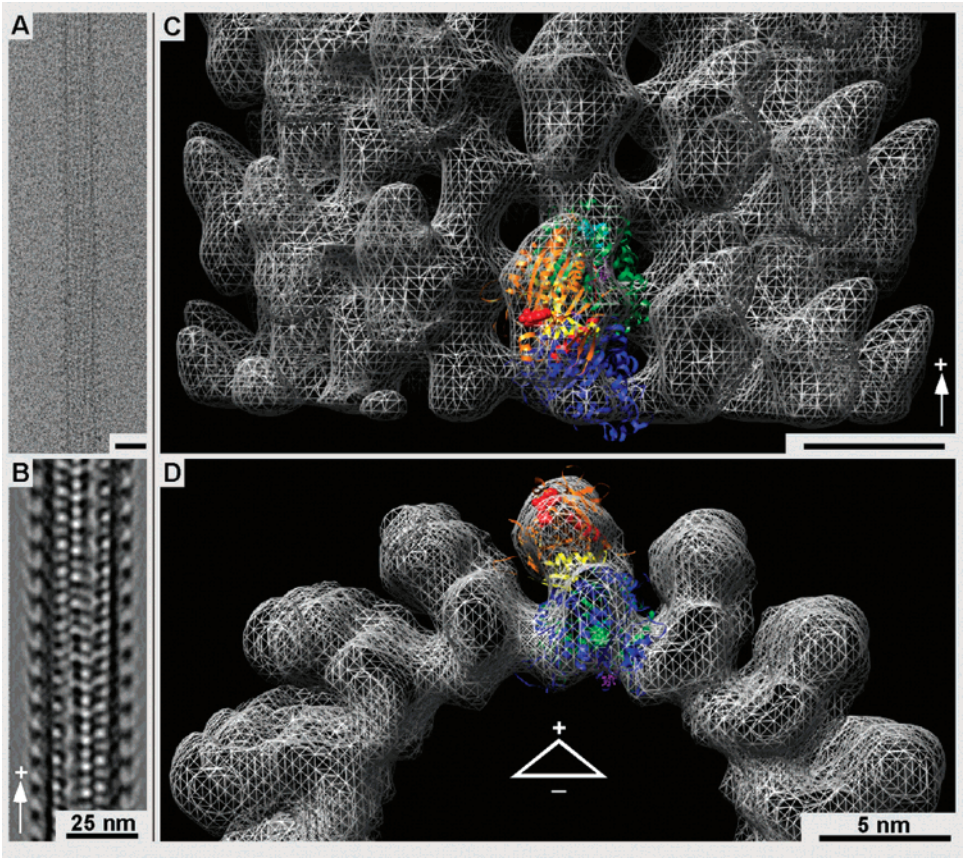

FIGURE 7: Helical reconstruction of NcKin3-434 complexed to microtubules in the presence of AMPPNP. (A) Raw-data image and (B) Fourier-filtered image of a complex between the motor domain and a 15-protofilament microtubule. (C) Large scale side-view and (D) end-on view of the helical 3-D map. The kinesin motor domain and the $\alpha\beta$-tubulin structure are docked into one position. The microtubule polarity is indicated in panels B, C, and D. Scale bars are equivalent in panels A and B and in panels C and D.

ing the structural similarity between Kif1A·AMPPCP and NcKin3·ADP—with regard to both the overall fold and the conformation of loop L9 and especially of S266/S215 (NcKin3/Kif1A)—it appears that the pre-isomerization or collision state (*32*) does not require the presence of the γ-phosphate. In this context, it is notable that the AMPPCP-like conformation had also been observed in the absence of AMPPCP (*31*). This provides an explanation as to why the NcKin3 motor domain can adopt the same conformation with ADP at the nucleotide binding side.

Nucleotide Binding Site. When one compares the sequences of kinesins, one observes a highly conserved motif (RxRP) that is involved in the binding of the nucleotide. It is notable that in NcKin3, the conserved proline is replaced by alanine (A48). Replacement of the bulky proline side group by a methyl group allows the adenine moiety to rotate out of its usual plane while ribose and phosphates stay in their normal places. This rotation weakens the stacking interaction with Y152 and leads to the loss of interactions between the adenine base and the loop L3. This should result in a reduced nucleotide binding affinity as compared to other kinesins with a canonical RxRP motif such as Kif1A and conventional kinesin (cf. Figure 1).

The solvent exposed structural elements surrounding the binding site of the adenine moiety, helix α0 and the loops L3 and L5, are among the regions of NcKin3 that deviate most from all known structures of Kif1A. Loop L3 and helix α0 are both displaced by about 4 Å, as compared to Kif1A·L5, and the insert loop in helix α2 is two amino acids shorter than in most other kinesins. These alterations are obviously caused by differences on the level of the primary structure rather than by artificial crystal contacts: as to the loop L3, a proline that is present in Kif1A (P62) but absent in the NcKin3 sequence, seems to be responsible for the rearrangement of the C_α trace. Relocation of helix α0 is mainly caused by loop L14 between β8 and α6. This tight loop of typically five amino acids is further shortened to three amino acids in NcKin3, resulting in modified H-bonding with α0.

Helix α0 and loop L14 are both adjacent to the N-terminal lobe (i.e., strands β1a, -b, -c and the interconnecting loops). The size and conformation of the β1b-L2-β1c region vary considerably between different types of kinesin. In NcKin3, loop L2 has a long insert as compared to conventional kinesins and Kif1A (Figure 1B). This insert is mostly disordered in the crystal structure. CryoEM of microtubules decorated with NcKin3-434 (Figure 8B) places the flexible end of loop L2 at the lower side of the motor domain (pointing to the minus end), a distance of about 1.5−2 nm above the surface of α-tubulin (see Figure 8B). This distance can easily be covered by the stretch of 15 amino acids that is not resolved by crystal structure analysis. Also, the presence of four arginines makes this missing stretch of loop L2 a potential candidate for tubulin binding. The image reconstruction shows enough electron density between L2 and the microtubule wall to accommodate the flexible loops L2 and L11. Because of its vicinity to helix α0 and the nucleotide binding site at one end, and the microtubule surface on the other end, loop L2 in NcKin3 could serve as

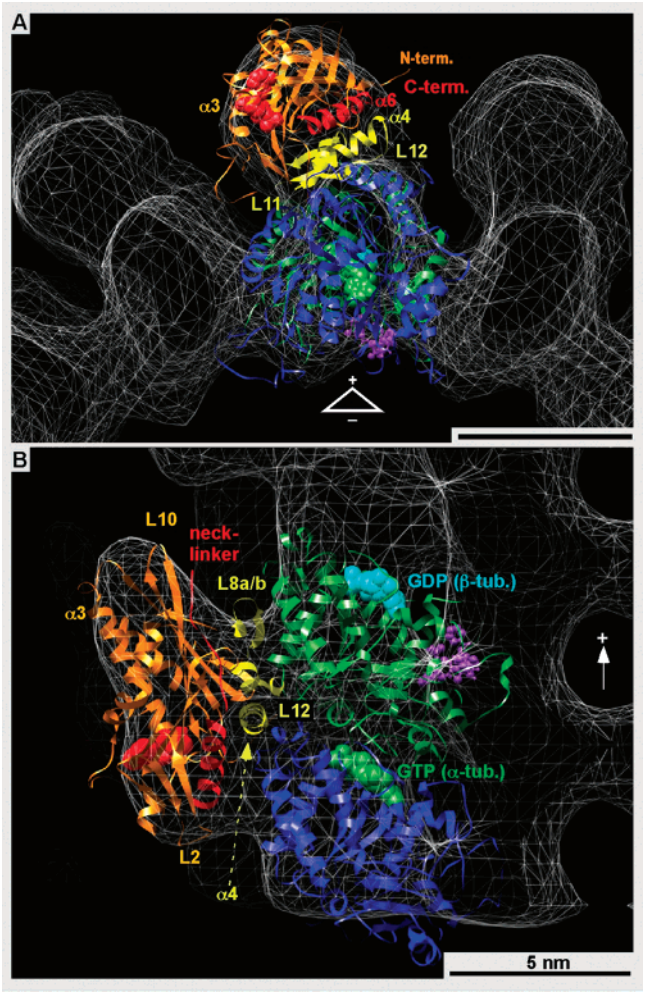

FIGURE 8: Docking of the NcKin3-434 X-ray structure into the EM-derived 3-D map. (A) End-on view of the microtubule-motor complex with the minus end oriented to the observer. Helix α4 is highlighed in yellow. The pink molecule at the bottom of tubulin is taxol (*68*, *74*). (B) Slightly tilted sideview of the motor-dimer complex with the microtubule plus end at the top. Helix α4 is located very close to the gap between α- and *β*-tubulin. Loops L2, L10, L11, and L12 are all invisible in the X-ray structure, but there seems to be enough room within the EM density to accommodate them. Loop L12 appears to play a crucial role in the interaction with the *β*-tubulin C-terminal end. The nucleotide shown in the motor molecule is that of the crystal structure (ADP), whereas AMPPNP was used for EM reconstruction of the microtubule-motor complex. The X-ray structure can be docked to the EM-derived electron density map as it corresponds to an ATP-like state, although ADP is bound in the active center. Small conformational changes in the motor molecule induced by microtubule binding cannot be excluded due to the limited resolution of the EM reconstruction.

an additional communication pathway between the nucleotide pocket and the microtubule binding site.

Fundamental Asymmetry of the Wild-Type Dimeric Motor. Kinetic dissection of the mechanochemical cycle revealed that wild-type dimeric NcKin3 moves in a non-processive manner with one head active and the other one permanently passive (*30*). Although not directly involved in ATP hydrolysis, the passive head is essential for detachment from the microtubule surface after hydrolysis. The structural basis for this asymmetry is unclear. Characterization of C-terminally truncated constructs showed that NcKin3 molecules dimerize via the interaction of a predicted coiled-coil region (residues ~434−513) that follows the neck linker, similar to conventional kinesin; the sequence of the coiled-coil, however, is much different from that of human HsKif5B (*30*). Remarkably, the last three heptads at the distal end of this region are required for dimerization.

Thus, wild-type NcKin3 is a dimeric motor that exhibits a fundamental asymmetry: there is an active head and a passive head, and the two heads do not exchange their roles over a long period of time. Such behavior of a dimer consisting of two identical protomers can be explained either by permanent structural asymmetry or by dynamic perpetuation of the initial roles the motor domains chose at the time they attached to a microtubule. In the latter case, the mechanochemical pathway must be narrow, such that role swapping does not occur. Conventional kinesin can probably serve as an example for the dynamic type of asymmetry: the essential interaction responsible for dimerization is the formation of a symmetric coiled-coil by the neck helices, yet there is growing evidence that conventional kinesin uses an asymmetric hand-over-hand mechanism (*11*−*14*, *36*). This asymmetry, however, is less fundamental than that of NcKin3 insofar as both motor domains are active and force producing, and only the details of the kinetic pathways followed by each head may be different.

Another example is the minus end directed motor Ncd, where high-resolution structures of symmetric and asymmetric conformations are available (PDB− IDs 1cz7, 2ncd, and 1n6 m (*20*, *44*, *45*)). As in conventional kinesin, the permanent interactions responsible for stable dimer formation are those within the symmetric coiled-coil of the neck-stalk helices. In contrast to conventional kinesin, however, Ncd proceeds in a nonprocessive manner using a powerstroke mechanism (*18*−*20*). This involves complete detachment once per cycle and allows the two heads to behave equivalently on average.

In the case of wild-type NcKin3, there is no indication that the second head ever contributes directly to microtubule-stimulated ATP hydrolysis, although NcKin3—like Ncd—most likely uses a power stroke mechanism (*30*). Hence, the asymmetric behavior of the protomers is probably not caused by a narrow kinetic pathway but rather due to a permanent structural asymmetry. The predicted coiled-coil domain (residues 435−513) must play an important role since C-terminally truncated constructs that contain the entire coiled-coil domain are dimeric, while shorter constructs are monomeric in solution (*30*). This region is certainly required for stabilization of the dimer. However, it is less obvious as to whether it is also responsible for the fundamental asymmetry of the dimer. Theoretically, the coiled-coil formation of homodimers should be less favorable for asymmetric conformations because of the inevitable mismatch at the ends: coiled-coils are usually blunt ended (*69*). Thus, it seems that the head/neck-linker domain also contributes to the fundamental asymmetry of NcKin3, possibly by triggering an asymmetric dimerization of the coiled-coil.

Asymmetric Interactions of the Motor Domains. There are only two types of tight intermolecular contacts in the crystal that potentially could be representative for the interactions under physiological conditions: a symmetric interaction of the (A, C) type and an asymmetric interaction of the [B, C] type. In the asymmetric arrangement represented by [B, C], the two motor domains approach each other in a way that is reminiscent of the dimers known from conventional kinesin

(*41*). In this arrangement, the neck linkers converge, so that their ends are in close contact with each other forming hydrogen bonds between Q421 of molecule B (backbone and side chain) and the backbone of A417 and V419 in molecule C. Such an arrangement would be consistent with dimerization via the interaction of the predicted coiled-coil sequence that follows the neck linker. Remarkably, the contacts between the neck linkers are out-of-register. This could result in an asymmetric association of the neck helices. This view is somewhat speculative, as the real structure of a dimeric NcKin3 construct is unknown. However, the possibility that the trigger sequence responsible for the asymmetric association of the neck helices could reside in the head/neck-linker domain adds plausibility to this hypothesis.

In the crystal structure of NcKin3-434, the asymmetric interaction between molecules B and C is tightened by the N-terminal extension of molecule C (Figure 6A). Most of the extension is invisible, but four residues immediately preceding the motor domain touch the other molecule (B), forming a kind of a hook where the side chain of R414 in the neck linker of the same molecule can bind. Thus, the N-terminal extension in one molecule appears to contribute to the association of the heads and at the same time secures the neck linker of that molecule in a docked conformation. However, docking of the neck linker is not strictly dependent on the intramolecular interaction between R414 and the N-terminal extension because this type of interaction does not exist in the other molecule. Furthermore, measurements of the microtubule-stimulated steady-state ATPase rate and activation constant suggest that a construct lacking the N-terminal extension has similar kinetic properties as NcKin3 constructs that are not truncated at the N-terminus (*30*). The function of the N-terminal extension is not yet known. Although the kinetic experiments show that the N-terminal extension is not required for the formation of NcKin3 dimers under normal conditions, it could still have a role in stabilizing the dimer.

Microtubule Binding Geometry. The 3-D EM map revealed a motor head structure that shows most of the characteristic features known from other kinesins (Figure 7C,D). The overall head structure has the typical wider but flatter shape toward the minus end and a higher but narrower appearance around loop L10, pointing toward the plus end. A structural feature that is more pronounced than in other reconstructions (e.g., see NcKIN-355 (*43*, *70*) and rKIN-354 (*34*)) is the separation of the overall head structure into two distinct lobes. At first glance, their presence might indicate a slightly flexible microtubule-binding conformation (e.g., see ref *34*). However, the lobes match the shape of the X-ray structure very tightly (see Figure 8). Hence, this feature seems real. As compared to Kinesin-1, the head appears to be slightly tilted to the right (clockwise) with respect to the protofilament axis when pointing upward to the plus end. This orientation corresponds well with the rotation seen for KIF1A-ADP (*31*), but the conformation seems opposite to the rotation that has been observed for rK354-AMPPNP (*34*) with respect to its nucleotide-free conformation. Note that the NcKin3-434-microtubule complex has been obtained in the presence of AMPPNP, an ATP analogue, and that the crystal structure of the NcKin3-434·ADP complex resembles an ATP-bound rather than an ADP-bound conformation. Thus, it seems allowed to dock the NcKin3-434 crystal structure into the electron density of the microtubule complex, although a microtubule-induced rearrangement of key structural elements cannot be excluded.

Switch II helix α4 is located close to the α−β intra-dimer tubulin interface but seems to maintain most of its contact with helix 12 of β-tubulin (Figure 8B). While the α-tubulin C-terminal end is too far from the kinesin head domain, the (invisible) β-tubulin C-terminus (co-located with the L12 label in Figure 8B) appears to play a crucial role with possible interactions to NcKin3 α4, α5 and loop L12. Region β5a,b-L8 touches the microtubule surface near the loop between β-tubulin helices H11 and H12 (Figure 8B). The EM map shows ample density at the region where loops L2, L11, and L12 would be expected to touch the outer tubulin surface. Loop L2 could well fill the apparent gap between the atomic structures of NcKin3-434 and tubulin. There is sufficient EM density present to accommodate that loop, which, with four arginines, may be a good candidate for making contact with α-tubulin helices H11 and H12 of α-tubulin at that location. However, it should be kept in mind that protein−ligand interactions can cause substantial rearrangements in the individual components. Thus, at the limited resolution of the EM reconstruction, it cannot be excluded that relocation of other parts of the motor-tubulin complex can account for the unassigned electron density.

Role of the Passive Head. Kinetic analysis suggested that NcKin3 uses a power stroke mechanism similar to Ncd. In the case of Ncd, the neck linker is part of a continuous and rigid coiled-coil, whereas in NcKin3, the neck linker seems to be flexible as in other N-type kinesin motors. Assuming a power stroke mechanism with the coiled-coil region as a lever arm then requires that the neck linker be locked in a rigid conformation, most likely by interaction with the passive head. Thus, the passive head in combination with the neck linker(s) could serve as a force- or torque-transducing mechanical element.

According to the findings by Adio et al. (*30*), the last three heptads of the coiled-coil are required for dimerization. At first glance, this argues that the distal end of the coiled-coil harbors essential interactions that are responsible for the particular form of kinetic asymmetry of NcKin3. Alternatively, an asymmetric interaction of the motor domains similar to the [B, C] interaction observed in the crystal could trigger dimerization in a way that leads to an asymmetric, sticky ended coiled-coil. Since sticky ends are energetically unfavorable, the requirement of the last three heptads could simply mean that a shorter coiled-coil would not suffice for stable and irreversible dimerization. In conclusion, the fundamental asymmetry of the wild-type NcKin3 motor and its kinetic properties seems to be the consequence of a cooperative phenomenon that relies on a trigger signal for dimerization by asymmetric head−neck contacts as well as an extended coiled-coil interaction for stabilization.

ACKNOWLEDGMENT

We thank the X13 consortium (University of Hamburg and EMBL Outstation Hamburg) for synchrotron beam time, in particular, Drs. M. Perbandt and W. Rypniewski for helpful discussions, Dan Wu for protein preparation, and Linda Sandblad (EMBL Heidelberg) for processing the EM data.

SUPPORTING INFORMATION AVAILABLE

Figure showing phase−amplitude plots of selected layer-lines of the helically reconstructed HcKIN-434 microtubule complex. This material is available free of charge via the Internet at http://pubs.acs.org.

REFERENCES

1. Lawrence, C. J., Dawe, R. K., Christie, K. R., Cleveland, D. W., Dawson, S. C., Endow, S. A., Goldstein, L. S., Goodson, H. V., Hirokawa, N., Howard, J., Malmberg, R. L., McIntosh, J. R., Miki, H., Mitchison, T. J., Okada, Y., Reddy, A. S., Saxton, W. M., Schliwa, M., Scholey, J. M., Vale, R. D., Walczak, C. E., and Wordeman, L. (2004) A standardized kinesin nomenclature, *J. Cell Biol. 167*, 19−22.
2. Dagenbach, E. M., and Endow, S. A. (2004) A new kinesin tree, *J. Cell Sci. 117*, 3−7.
3. Hackney, D. D. (1995) Highly processive microtubule-stimulated ATP hydrolysis by dimeric kinesin head domains, *Nature (London, U.K.) 377*, 448−450.
4. Howard, J., Hudspeth, A. J., and Vale, R. D. (1989) Movement of microtubules by single kinesin molecules, *Nature (London, U.K.) 342*, 154−158.
5. Valentine, M. T., and Gilbert, S. P. (2007) To step or not to step? How biochemistry and mechanics influence processivity in kinesin and Eg5, *Curr. Opin. Cell Biol. 19*, 1−7.
6. Coy, D. L., Wagenbach, M., and Howard, J. (1999) Kinesin takes one 8-nm step for each ATP that it hydrolyzes, *J. Biol. Chem. 274*, 3667−3671.
7. Hua, W., Young, E. C., Fleming, M. L., and Gelles, J. (1997) Coupling of kinesin steps to ATP hydrolysis, *Nature (London, U.K.) 388*, 390−393.
8. Schnitzer, M. J., and Block, S. M. (1997) Kinesin hydrolyses one ATP per 8-nm step, *Nature (London, U.K.) 388*, 386−390.
9. Gilbert, S. P., Moyer, M. L., and Johnson, K. A. (1998) Alternating site mechanism of the kinesin ATPase, *Biochemistry 37*, 792−799.
10. Hackney, D. D. (1994) Evidence for alternating head catalysis by kinesin during microtubule-stimulated ATP hydrolysis, *Proc. Natl. Acad. Sci. U.S.A. 91*, 6865−6869.
11. Yildiz, A., Tomishige, M., Vale, R. D., and Selvin, P. R. (2004) Kinesin walks hand-over-hand, *Science (Washington, DC, U.S.) 303*, 676−678.
12. Asbury, C. L., Fehr, A. N., and Block, S. M. (2003) Kinesin moves by an asymmetric hand-over-hand mechanism, *Science (Washington, DC, U.S.) 302*, 2130−2134.
13. Higuchi, H., Bronner, C. E., Park, H. W., and Endow, S. A. (2004) Rapid double 8-nm steps by a kinesin mutant, *EMBO J. 23*, 2993−2999.
14. Kaseda, K., Higuchi, H., and Hirose, K. (2003) Alternate fast and slow stepping of a heterodimeric kinesin molecule, *Nat. Cell Biol. 5*, 1079−1082.
15. Tomishige, M., Stuurman, N., and Vale, R. D. (2006) Single-molecule observations of neck linker conformational changes in the kinesin motor protein, *Nat. Struct. Mol. Biol. 13*, 887−894.
16. Skiniotis, G., Surrey, T., Altmann, S., Gross, H., Song, Y. H., Mandelkow, E., and Hoenger, A. (2003) Nucleotide-induced conformations in the neck region of dimeric kinesin, *EMBO J. 22*, 1518−1528.
17. Carter, N. J., and Cross, R. A. (2006) Kinesin's moonwalk, *Curr. Opin. Cell Biol. 18*, 61−67.
18. Wendt, T. G., Volkmann, N., Skiniotis, G., Goldie, K. N., Muller, J., Mandelkow, E., and Hoenger, A. (2002) Microscopic evidence for a minus-end-directed power stroke in the kinesin motor Ncd, *EMBO J. 21*, 5969−5978.
19. Endres, N. F., Yoshioka, C., Milligan, R. A., and Vale, R. D. (2006) A lever-arm rotation drives motility of the minus-end-directed kinesin Ncd, *Nature (London, U.K.) 439*, 875−878.
20. Yun, M., Bronner, C. E., Park, C. G., Cha, S. S., Park, H. W., and Endow, S. A. (2003) Rotation of the stalk/neck and one head in a new crystal structure of the kinesin motor protein, Ncd, *EMBO J. 22*, 5382−5389.
21. Okada, Y., Yamazaki, H., Sekine-Aizawa, Y., and Hirokawa, N. (1995) The neuron-specific kinesin superfamily protein KIF1A is a unique monomeric motor for anterograde axonal transport of synaptic vesicle precursors, *Cell 81*, 769−780.
22. Pierce, D. W., Hom-Booher, N., Otsuka, A. J., and Vale, R. D. (1999) Single-molecule behavior of monomeric and heteromeric kinesins, *Biochemistry 38*, 5412−5421.
23. Okada, Y., and Hirokawa, N. (2000) Mechanism of the single-headed processivity: Diffusional anchoring between the K-loop of kinesin and the C-terminus of tubulin, *Proc. Natl. Acad. Sci. U.S.A. 97*, 640−645.
24. Al-Bassam, J., Cui, Y., Klopfenstein, D., Carragher, B. O., Vale, R. D., and Milligan, R. A. (2003) Distinct conformations of the kinesin Unc104 neck regulate a monomer to dimer motor transition, *J. Cell Biol. 163*, 743−753.
25. Rashid, D. J., Bononi, J., Tripet, B. P., Hodges, R. S., and Pierce, D. W. (2005) Monomeric and dimeric states exhibited by the kinesin-related motor protein KIF1A, *J. Pept. Res. 65*, 538−549.
26. Shimizu, Y., Morii, H., Arisaka, F., and Tanokura, M. (2005) Stalk region of kinesin-related protein Unc104 has a moderate ability to form coiled-coil dimer, *Biochem. Biophys. Res. Commun. 337*, 868−874.
27. Tomishige, M., Klopfenstein, D. R., and Vale, R. D. (2002) Conversion of Unc104/KIF1A kinesin into a processive motor after dimerization, *Science (Washington, DC, U.S.) 297*, 2263−2267.
28. Schoch, C. L., Aist, J. R., Yoder, O. C., and Turgeon, B. G. (2003) A complete inventory of fungal kinesins in representative filamentous ascomycetes, *Fungal Genet. Biol. 39*, 1−15.
29. Fuchs, F., and Westermann, B. (2005) Role of Unc104/KIF1-related motor proteins in mitochondrial transport in *Neurospora crassa*, *Mol. Biol. Cell 16*, 153−161.
30. Adio, S., Bloemink, M., Hartel, M., Leier, S., Geeves, M. A., and Woehlke, G. (2006) Kinetic and mechanistic basis of the non-processive kinesin-3 motor NcKin3, *J. Biol. Chem. 281*, 37782−37793.
31. Kikkawa, M., Sablin, E. P., Okada, Y., Yajima, H., Fletterick, R. J., and Hirokawa, N. (2001) Switch-based mechanism of kinesin motors, *Nature (London, U.K.) 411*, 439−445.
32. Nitta, R., Kikkawa, M., Okada, Y., and Hirokawa, N. (2004) KIF1A alternately uses two loops to bind microtubules, *Science (Washington, DC, U.S.) 305*, 678−683.
33. Hirose, K., Lowe, J., Alonso, M., Cross, R. A., and Amos, L. A. (1999) Congruent docking of dimeric kinesin and ncd into three-dimensional electron cryomicroscopy maps of microtubule−motor ADP complexes, *Mol. Biol. Cell 10*, 2063−2074.
34. Skiniotis, G., Cochran, J. C., Muller, J., Mandelkow, E., Gilbert, S. P., and Hoenger, A. (2004) Modulation of kinesin binding by the C-termini of tubulin, *EMBO J. 23*, 989−999.
35. Klumpp, L. M., Brendza, K. M., Gatial, J. E., III, Hoenger, A., Saxton, W. M., and Gilbert, S. P. (2004) Microtubule−kinesin interface mutants reveal a site critical for communication, *Biochemistry 43*, 2792−2803.
36. Hoenger, A., Thormahlen, M., Diaz-Avalos, R., Doerhoefer, M., Goldie, K. N., Muller, J., and Mandelkow, E. (2000) A new look at the microtubule binding patterns of dimeric kinesins, *J. Mol. Biol. 297*, 1087−1103.
37. Rice, S., Lin, A. W., Safer, D., Hart, C. L., Naber, N., Carragher, B. O., Cain, S. M., Pechatnikova, E., Wilson-Kubalek, E. M., Whittaker, M., Pate, E., Cooke, R., Taylor, E. W., Milligan, R. A., and Vale, R. D. (1999) A structural change in the kinesin motor protein that drives motility, *Nature (London, U.K.) 402*, 778−784.
38. Sindelar, C. V., and Downing, K. H. (2007) The beginning of kinesin's force-generating cycle visualized at 9 Å resolution, *J. Cell Biol. 177*, 377−385.
39. Kull, F. J., Sablin, E. P., Lau, R., Fletterick, R. J., and Vale, R. D. (1996) Crystal structure of the kinesin motor domain reveals a structural similarity to myosin, *Nature (London, U.K.) 380*, 550−555.
40. Sack, S., Müller, J., Marx, A., Thormählen, M., Mandelkow, E. M., Brady, S. T., and Mandelkow, E. (1997) X-ray structure of motor and neck domains from rat brain kinesin, *Biochemistry 36*, 16155−16165.
41. Kozielski, F., Sack, S., Marx, A., Thormählen, M., Schönbrunn, E., Biou, V., Thompson, A., Mandelkow, E. M., and Mandelkow, E. (1997) The crystal structure of dimeric kinesin and implications for microtubule-dependent motility, *Cell 91*, 985−994.
42. Sindelar, C. V., Budny, M. J., Rice, S., Naber, N., Fletterick, R., and Cooke, R. (2002) Two conformations in the human kinesin power stroke defined by X-ray crystallography and EPR spectroscopy, *Nat. Struct. Biol. 9*, 844−848.

43. Song, Y. H., Marx, A., Müller, J., Woehlke, G., Schliwa, M., Krebs, A., Hoenger, A., and Mandelkow, E. (2001) Structure of a fast kinesin: Implications for ATPase mechanism and interactions with microtubules, *EMBO J. 20*, 6213−6225.
44. Kozielski, F., De Bonis, S., Burmeister, W. P., Cohen-Addad, C., and Wade, R. H. (1999) The crystal structure of the minus-end-directed microtubule motor protein ncd reveals variable dimer conformations, *Struct. Fold Des. 7*, 1407−1416.
45. Sablin, E. P., Case, R. B., Dai, S. C., Hart, C. L., Ruby, A., Vale, R. D., and Fletterick, R. J. (1998) Direction determination in the minus-end-directed kinesin motor Ncd, *Nature (London, U.K.) 395*, 813−816.
46. Yun, M., Zhang, X., Park, C. G., Park, H. W., and Endow, S. A. (2001) A structural pathway for activation of the kinesin motor ATPase, *EMBO J. 20*, 2611−2618.
47. Vinogradova, M. V., Reddy, V. S., Reddy, A. S., Sablin, E. P., and Fletterick, R. J. (2004) Crystal structure of kinesin regulated by Ca^{2+}/calmodulin, *J. Biol. Chem. 279*, 23504−23509.
48. Gulick, A. M., Song, H., Endow, S. A., and Rayment, I. (1998) X-ray crystal structure of the yeast Kar3 motor domain complexed with Mg•ADP to 2.3 Å resolution, *Biochemistry 37*, 1769−1776.
49. Marx, A., Müller, J., and Mandelkow, E. (2005) The structure of microtubule motor proteins, *Adv. Protein Chem. 71*, 299−344.
50. Vale, R. D., and Milligan, R. A. (2000) The way things move: Looking under the hood of molecular motor proteins, *Science (Washington, DC, U.S.) 288*, 88−95.
51. Kikkawa, M., and Hirokawa, N. (2006) High-resolution cryo-EM maps show the nucleotide binding pocket of KIF1A in open and closed conformations, *EMBO J. 25*, 4187−4194.
52. Itakura, S., Yamakawa, H., Toyoshima, Y. Y., Ishijima, A., Kojima, T., Harada, Y., Yanagida, T., Wakabayashi, T., and Sutoh, K. (1993) Force-generating domain of myosin motor, *Biochem. Biophys. Res. Commun. 196*, 1504−1510.
53. Otwinowski, Z., and Minor, W. (1997) Processing of X-ray diffraction data collected in oscillation mode, in *Methods in Enzymology, Vol. 276: Macromolecular Crystallography, Part A* (Carter, C. W., and Sweet, R. M., Eds.) pp 307−326, Academic Press, San Diego.
54. CCP4 (Collaborative Computer Project Number 4). (1994) The CCP4 Suite: Programs for protein crystallography, *Acta Crystallogr., Sect. D: Biol. Crystallogr. 50*, 760−763.
55. McCoy, A. J., Grosse-Kunstleve, R. W., Storoni, L. C., and Read, R. J. (2005) Likelihood-enhanced fast translation functions, *Acta Crystallogr., Sect. D: Biol. Crystallogr. 61*, 458−464.
56. Murshudov, G. N., Vagin, A. A., and Dodson, E. J. (1997) Refinement of macromolecular structures by the maximum-likelihood method, *Acta Crystallogr., Sect. D: Biol. Crystallogr. 53*, 240−255.
57. Emsley, P., and Cowtan, K. (2004) Coot: Model-building tools for molecular graphics, *Acta Crystallogr., Sect. D: Biol. Crystallogr. 60*, 2126−2132.
58. Brunger, A. T., Adams, P. D., Clore, G. M., DeLano, W. L., Gros, P., Grosse-Kunstleve, R. W., Jiang, J. S., Kuszewski, J., Nilges, M., Pannu, N. S., Read, R. J., Rice, L. M., Simonson, T., and Warren, G. L. (1998) Crystallography and NMR system: A new software suite for macromolecular structure determination, *Acta Crystallogr., Sect. D: Biol. Crystallogr. 54*, 905−921.
59. Laskowski, R. A., MacArthur, M. W., Moss, D. S., and Thornton, J. M. (1993) PROCHECK: A program to check the stereochemical quality of protein structures, *J. Appl. Crystallogr. 26*, 283−291.
60. Hooft, R. W., Vriend, G., Sander, C., and Abola, E. E. (1996) Errors in protein structures, *Nature (London, U.K.) 381*, 272.
61. Beuron, F., and Hoenger, A. (2001) Structural analysis of the microtubule−kinesin complex by cryo-electron microscopy, *Methods Mol. Biol. 164*, 235−254.
62. Dubochet, J., Adrian, M., Chang, J. J., Homo, J. C., Lepault, J., McDowall, A. W., and Schultz, P. (1988) Cryo-electron microscopy of vitrified specimens, *Q. Rev. Biophys. 21*, 129−228.
63. Hoenger, A., and Nicastro, D. (2007) Electron microscopy of microtubule-based cytoskeletal machinery, *Methods Cell. Biol. 79*, 437−462.
64. Whittaker, M., Carragher, B. O., and Milligan, R. A. (1995) PHOELIX: A package for semi-automated helical reconstruction, *Ultramicroscopy 58*, 245−259.
65. Schroeter, J. P., and Bretaudiere, J. P. (1996) SUPRIM: Easily modified image processing software, *J. Struct. Biol. 116*, 131−137.
66. Pettersen, E. F., Goddard, T. D., Huang, C. C., Couch, G. S., Greenblatt, D. M., Meng, E. C., and Ferrin, T. E. (2004) UCSF Chimera: A visualization system for exploratory research and analysis, *J. Comput. Chem. 25*, 1605−1612.
67. Kikkawa, M., Okada, Y., and Hirokawa, N. (2000) 15 Å resolution model of the monomeric kinesin motor, KIF1A, *Cell 100*, 241−252.
68. Nogales, E., Wolf, S. G., and Downing, K. H. (1998) Structure of the alpha beta tubulin dimer by electron crystallography, *Nature (London, U.K.) 391*, 199−203.
69. Woolfson, D. N. (2005) The design of coiled-coil structures and assemblies, *Adv. Protein Chem. 70*, 79−112.
70. Krebs, A., Goldie, K. N., and Hoenger, A. (2004) Complex formation with kinesin motor domains affects the structure of microtubules, *J. Mol. Biol. 335*, 139−153.
71. Chenna, R., Sugawara, H., Koike, T., Lopez, R., Gibson, T. J., Higgins, D. G., and Thompson, J. D. (2003) Multiple sequence alignment with the Clustal series of programs, *Nucleic Acids Res. 31*, 3497−3500.
72. Kabsch, W., and Sander, C. (1983) Dictionary of protein secondary structure: Pattern recognition of hydrogen-bonded and geometrical features, *Biopolymers 22*, 2577−2637.
73. DeLano, W. L. (2002) *The PyMOL Molecular Graphics System*, DeLano Scientific, San Carlos, CA, http://www.pymol.org.
74. Nogales, E., Whittaker, M., Milligan, R. A., and Downing, K. H. (1999) High-resolution model of the microtubule, *Cell 96*, 79−88.

BI701483H